Interpenetrating Three-Dimensional Diamondoid Lattices and Antiferromagnetic Ordering (T_c = 73 K) of $Mn^{II}(CN)_2$

Christopher M. Kareis,[†] Saul H. Lapidus,[‡] Peter W. Stephens,*,[§,‡] and Joel S. Miller*,[†]

[†]Department of Chemistry, 315 S. 1400 E. RM 2124, University of Utah, Salt Lake City, Utah 84112-0850, United States
[‡]Department of Physics & Astronomy, Stony Brook University, Stony Brook, New York 11794-3800, United States
[§]Photon Sciences Directorate, Brookhaven National Laboratory, Upton, New York 11973, United States

Ⓢ *Supporting Information*

ABSTRACT: Thermolysis of either the 3-D, bridged-layered $[NEt_4]Mn^{II}_3(CN)_7$ or 2-D, layered $[NEt_4]_2Mn^{II}_3(CN)_8$ forms $Mn^{II}(CN)_2$. Rietveld analysis of the high-resolution synchrotron powder X-ray diffraction data determined that $Mn^{II}(CN)_2$ is cubic [a = 6.1488(3) Å] (space group = $Pn\bar{3}m$) consisting of two independent, interpenetrating networks having the topology of the diamond lattice. Each tetrahedrally coordinated Mn^{II} is bonded to four orientationally disordered cyanide ligands. $Mn^{II}(CN)_2$ magnetically orders as an antiferromagnet with a T_c = 73 K determined from the peak in $d(\chi T)/dT$. Exchange coupling estimated via the mean field Heisenberg model from the transition temperature (J/k_B = −4.4 K) and low temperature magnetic susceptibility of the ordered phase (J/k_B = −7.2 K) indicate that $Mn^{II}(CN)_2$ experiences weak antiferromagnetic coupling. The discrepancy between those estimates is presumably due to local anisotropy at the Mn^{II} sites arising from the CN orientational disorder or interactions between the interpenetrating lattices.
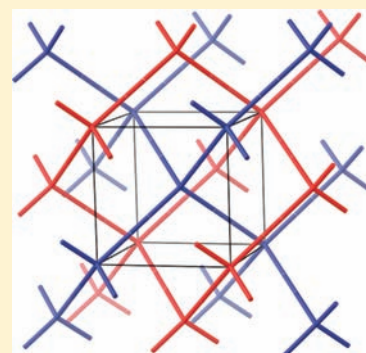
INTRODUCTION

Prussian blue structured hexacyanometalates can have $M'^{III}_4[M^{II}(CN)_6]_3$, $A^+M'^{II}[M^{III}(CN)_6]$, $M'^{II}_3[M^{III}(CN)_6]_2$, $A^+M'^{III}[M^{II}(CN)_6]$, $A^+_2M'^{II}[M^{II}(CN)_6]$, and $M'^{III}[M^{III}(CN)_6]$ (A^+ = cation) compositions that are typically hydrated.[1−3] This family of materials shares common structural features of (a) a face centered cubic (*fcc*) unit cell (~10.1 < a < ~10.5 Å), (b) low-spin C-bonded $[M(CN)_6]^{n−}$ surrounded by high spin M'^{II} (or M'^{III}) that is bonded to six cyanide nitrogens, and (c) linear —M′—N≡C—M—C≡N—M′— linkages along the three Cartesian axes, except where defect sites occur. Non-*fcc* related materials, based upon tetra-,[4−6] penta-,[7] hepta-,[8−10] and octacyanometalates[8,9,11] have also been reported. Due to the strong exchange among adjacent metal sites via the conjugated bridging cyanide,[12] these materials magnetically order, typically as ferrimagnets, with examples that have magnetic ordering temperatures, T_c, up to ~100 °C.[1−3]

Recently, we reported that the reaction of $A^+CN^−$ (A = Na, K, Rb) with $Mn(O_2CMe)_2$ forms $A^+_2Mn^{II}[Mn^{II}(CN)_6]$, which have monoclinic or rhombehedral unit cells, and the —M′—N≡C linkages are nonlinear with ∠M′—N≡C ranging from 142° to 153°, that is, substantially less than 180°.[13,14] Furthermore, while seeking $[NEt_4]_2Mn^{II}[Mn^{II}(CN)_6]$, $[NEt_4]$-$Mn^{II}_3(CN)_7·xMeOH$ (**1**)[15] and $[NEt_4]_2Mn^{II}_3(CN)_8·xH_2O$ (**2**)[15,16] were isolated and structurally characterized to have 3-D bridged-layered and 2-D layered structures, respectively. Herein, we report that the thermolysis of either **1** or **2** forms a material of $Mn^{II}(CN)_2$ composition.

A material of $Mn^{II}(CN)_2$ composition has been reported from the reaction of $[PPN]_2[Mn^{II}(CN)_4]$ (PPN = Ph_3P=N=

PPh_3^+) and $[Mn(NCMe)_6][TFPB]_2$ {TFPB = B-$[C_6H_3(CF_3)_2]_4^−$}. This was proposed to have an interpenetrating diamondoid structure, akin to $M(CN)_2$ (M = Zn, Cd),[6] and to order as an antiferromagnet at 65 K.[4,5] Material synthesized by the thermolysis of **1** and **2** yields a higher quality material than what is produced by the solution route. This work validates the proposed structure, clarifies details via high-resolution synchrotron powder X-ray diffraction data, and reports the magnetic behavior in greater detail.

EXPERIMENTAL SECTION

$[NEt_4]Mn^{II}_3(CN)_7·xMeOH$ (**1**) and $[NEt_4]_2Mn^{II}_3(CN)_8·xH_2O$ (**2**) were prepared as previously reported.[15,16] All manipulations of the materials were performed in an oxygen-free (<1.0 ppm O_2) wet or drybox.

Physical Methods. Infrared spectra were recorded from 400 to 4000 cm$^{−1}$ on a Bruker Tensor 37 spectrometer (±1 cm$^{−1}$) as KBr pellets or Nujol mulls. Thermogravimetric analyses (TGA) with mass spectroscopic (MS) analysis of the gaseous products were performed with a TA Model Q500 TGA equipped with a Pfeiffer Thermostar GSD301T3 quadrupole mass spectrometer to identify gaseous products with masses less than 300 amu. Experiments were performed in a Vacuum Atmospheres DriLab under nitrogen to protect air- and moisture-sensitive samples. Samples were placed in an aluminum pan and heated at 5 °C/min under a continuous 10-mL/min-nitrogen flow.

Magnetic susceptibilities were measured in a 1000 Oe applied field between 5 and 300 K on a Quantum Design 5T MPMS superconducting quantum interference device (SQUID) equipped

with a reciprocating sample measurement system, low field option, and continuous low temperature control with enhanced thermometry features, as previously described.[17] Powder samples for magnetic measurements were loaded in gelatin capsules. The DC magnetization temperature dependence was obtained by cooling in zero field, and then data was collected on warming. AC susceptibilities were measured at 33, 100, and 1000 Hz. On the basis of Pascal's constants, the core diamagnetic correction is -40×10^{-6} emu/mol for the sample used in magnetic studies.

Powder diffraction measurements for the structure analysis were performed at beamline X16C of the National Synchrotron Light Source at Brookhaven National Laboratory. The powdered samples were held in a 1.0 mm diameter thin-wall quartz capillary. X-rays of wavelength 0.69994(3) Å were selected by a Si(111) channel cut monochromator. Diffracted X-rays were selected by a Ge(111) analyzer and detected by a scintillation counter. The incident intensity was monitored by an ion chamber and used to normalize the measured signal. The TOPAS-Academic program was used to study and refine the crystal structures.[18]

$Mn^{II}(CN)_2$. 1 or 2 was placed into a thick-walled Schlenck tube, and care was taken to ensure that the sample and reaction vessel remained horizontal. The tube was then wrapped with 0.5 in. heat tape with a thermocouple between the heater and flask close to the sample. The tube was then heated, in a six-step manner starting at 50 °C, and increasing the temperature by 50 °C every 30 min until reaching 300 °C, at which time the temperature was increased by 80 °C and held there for 1 h while under dynamic vacuum of ~60 mTorr. The tube was then allowed to cool to room temperature, and the resulting off-white solid was collected. The material is very electrostatic and is difficult to handle. Yield: 40 mg (90%) based on Mn.

■ RESULTS AND DISCUSSION

The thermal properties of $[NEt_4]Mn^{II}_3(CN)_7 \cdot x$MeOH (**1**) and $[NEt_4]_2Mn^{II}_3(CN)_8 \cdot xH_2$O (**2**) were analyzed by thermogravimetric analyses (Figure 1) with mass spectroscopic analysis (TGA/MS) of the volatized products. Heating **1** shows a 7.00% and 31.24% mass loss at ~200 and 300 °C, respectively, that are due to the sequential loss of 1.3 equiv of MeOH and 1 equiv of [Et$_4$N]CN. Likewise, thermolysis of **2** shows a 0.70% and 52.95% mass loss at ~170 and ~250 °C, respectively. This was analyzed to be the sequential loss of 0.5 equiv of H$_2$O followed by 2 equiv of [Et$_4$N]CN. In both, the total mass loss, 38.24 and 53.65% for **1** and **2**, respectively, below 400 °C, indicated that the thermolysis product had a molecular mass of ~319 g/mol for **1** and 298 g/mol for **2**. These results suggested that the solid was $Mn_3(CN)_6$ {= $Mn(CN)_2$}.

The IR spectra of the thermolysis products of both **1** and **2** were identical and exhibit a single, sharp, intense ν_{CN} absorption at 2174 cm^{-1}, slightly shifted from the previously reported value (2170 cm^{-1}) for Mn(CN)$_2$.[4]

Single crystals suitable for X-ray analysis were not available due to the fine particulate nature of the thermolysis product. Nonetheless, the material exhibited clear powder X-ray diffraction (PXRD) patterns, enabling the structure to be determined by synchrotron PXRD (Figure 2).[19] It has a cubic unit cell [a = 6.1488(3) Å]. The fact that the parent materials contain Mn(CN)$_4$ units and the similarity of typical Mn−C−N−Mn distances to half of the body diagonal suggest that the structure is similar to M(CN)$_2$ (M = Cd, Zn) with a double diamond-type lattice,[6] and the preliminary model suggested for Mn(CN)$_2$. In this model, there are Mn ions located at the origin and the body center of the unit cell. The Mn at the body center is connected by CN linkages to four corner sites: [000], [110], [101], and [011]. While crystallographically equivalent, the other four corners of the unit cell are part of a second, independent diamond lattice. There are two possible space
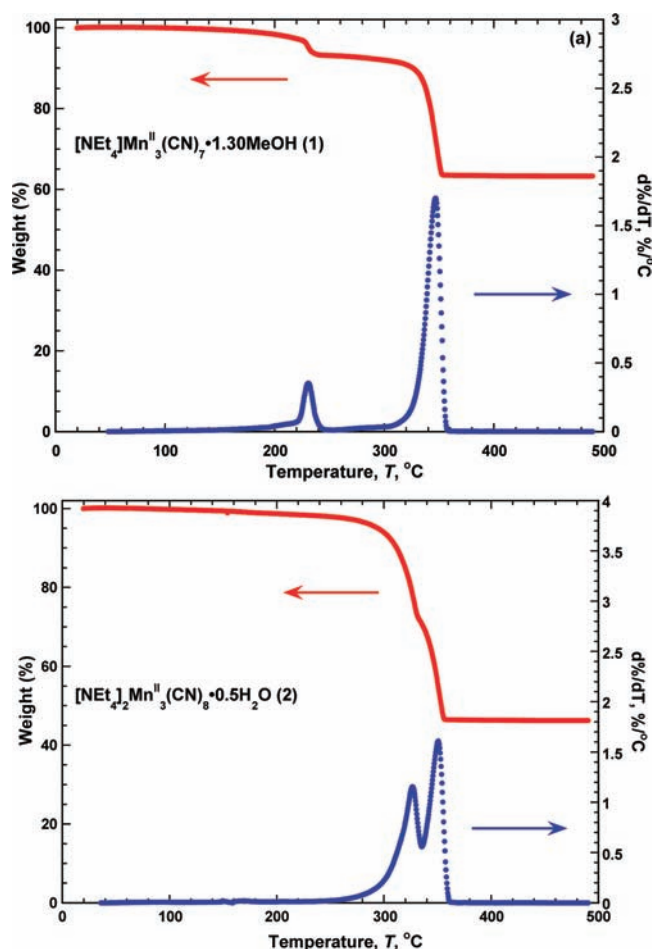
Figure 1. TGA traces for **1** (a) and **2** (b). The top trace in each plot is the TGA, and its derivative is on the bottom.

groups for this structure; in $Pn\bar{3}m$ the corner and body center Mn sites are equivalent and the nitriles are orientationally disordered, whereas $P\bar{4}3m$ has two distinct metal sites and allows for the possibility of ordered nitriles. The PXRD measurements do not directly distinguish between these two models, but $Pn\bar{3}m$ is much more likely as trial refinements in $P\bar{4}3m$ converge to identical Mn−C and Mn−N bond lengths within the standard uncertainty of 0.01 Å. Finally, powder neutron diffraction measurements on Zn(CN)$_2$ are able to distinguish C from N and reveal that that material has the disordered $Pn\bar{3}m$ structure.[6b]

A summary of crystallographic parameters for Mn(CN)$_2$ is provided in Table 1. The structure consists of interpenetrating diamond-like lattices composed of Mn^{II} ions tetrahedrally bound to disordered CN$^-$ ions, Figure 3. The Mn^{II} ions occupy a single Wyckoff position, and the C and N atoms are disordered between two equivalent sites on the threefold axis that connects the two nearest Mn^{II} ions on each sublattice. Due to the orientational disorder, the Mn−C and Mn−N distances are identical and are 2.081(2) Å. Presumably, individual Mn−C bonds are shorter and Mn−N bonds longer, but those differences are masked by the disorder. In particular, it is important to note that most of the Mn^{II} ions have a point symmetry lower than the $\bar{4}3m$ crystallographic site symmetry. The Mn−N≡C angles are 180°. The intra- and inter-sublattice Mn···Mn separations are both 5.3250(3) Å.
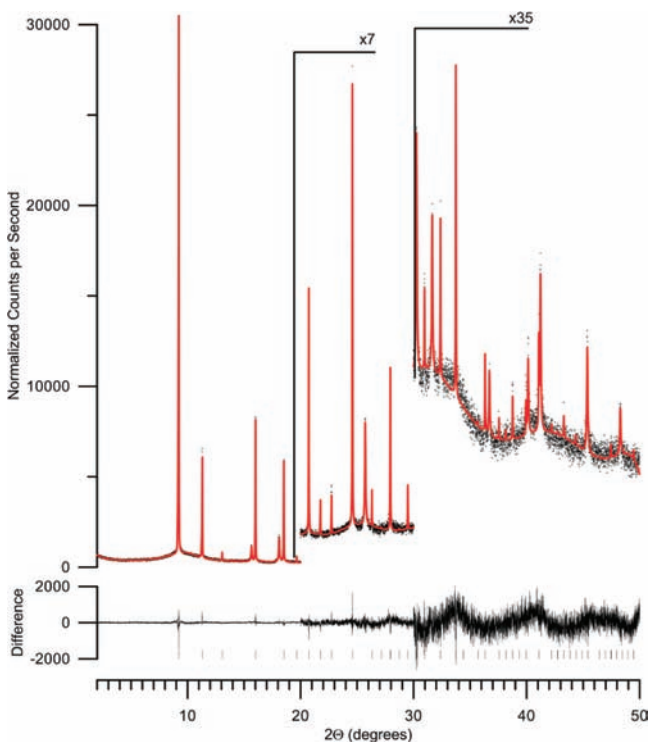
Figure 2. High-resolution synchrotron PXRD (dots) and Rietveld fit (line) of the data for $Mn(CN)_2$. The lower traces for each plot are the differences, measured − calculated, plotted to the same vertical scale.

Table 1. Summary of Crystallographic Parameters for $Mn(CN)_2$

	$Mn(CN)_2$
formula	C_2MnN_2
MW, g/mol	107.03
a, Å	6.1488(3)
V, Å^3	232.47(3)
Z	2
space group	$Pn\bar{3}m$
ρ_{calcd}, g/cm^3	1.529
R_{wp} ^{a,b}	5.917
R_{exp} ^{b,c}	4.809
T, K	298
GOF (R_{wp}/R_{exp})	1.230

$^a R_{wp} = \{[\sum_i w_i(y_i^{calcd} - y_i^{obs})^2]/[\sum_i w_i(y_i^{obs})^2]\}^{1/2}$. $^b y_i^{calcd}$ and y_i^{obs} are the calculated and observed intensities at the ith point in the profile, normalized to monitor intensity. The weight w_i is $1/\sigma^2$ from the counting statistics, with the same normalization factor. N is the number of points in the measured profile minus the number of parameters. $^c R_{exp} = \{N/[\sum_i w_i(y_i^{obs})^2]\}^{1/2}$

The magnetic susceptibility, χ, of $Mn(CN)_2$ was measured from 5 to 300 K, and is plotted as $\chi T(T)$, $\chi^{-1}(T)$ (Figure 4), and $\chi(T)$ (Figure 5). $Mn(CN)_2$ has a room temperature χT value of 3.41 emu K/mol-Mn that gradually decreases as the temperature is reduced. The room temperature value of χT is greater than the previously reported value of 2.42 emu K/mol[4] but is still significantly reduced from the predicted spin-only value of 4.375 emu K/mol per $S = {}^5/_2$ Mn^{II}. The reduced room-temperature χT value is in accord with strong antiferromagnetic coupling. Between 135 K and ambient temperature, $\chi^{-1}(T)$ is linear, following the Curie−Weiss equation, $\chi = C(T - \theta)^{-1}$ with $C = 5.8$ emu mol^{-1} K^{-1} and $\theta = -215$ K. The observed
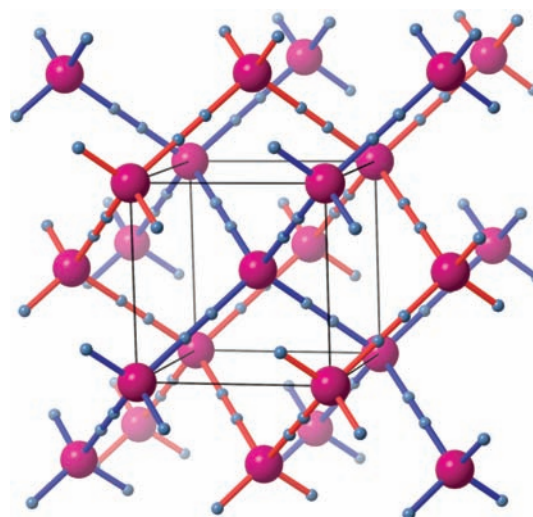
Figure 3. Structure of $Mn(CN)_2$ (Mn is maroon; C and N are disordered and are blue). One diamond sublattice has red bonds, and the other interpenetrating lattice has blue bonds.
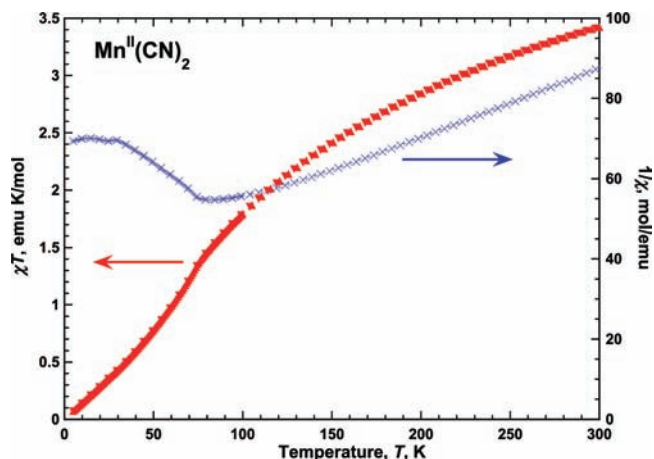
Figure 4. $\chi T(T)$ (▲,▼) and $\chi^{-1}(T)$ (+, ×) for $Mn(CN)_2$ in a 1000 Oe applied field. Data taken on cooling: ×, ▼; data taken on heating: +, ▲.
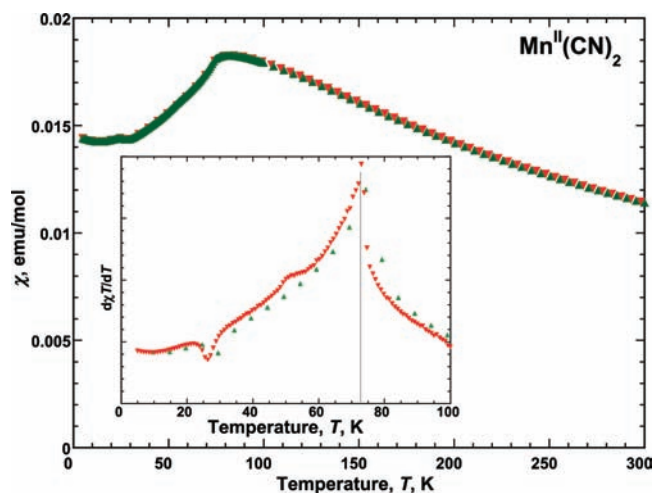
Figure 5. $\chi(T)$ and $d\chi T/dT$ (inset) for $Mn(CN)_2$ in a 1 kOe applied field. Data taken on cooling: ▼; data taken on heating: ▲.

value of C is in fair agreement with the value 4.4 calculated for g = 2, S = 5/2, indicating that, indeed, the Mn[II] ions are high-spin. Lower temperature deviations from the Curie−Weiss equation cannot be explained by a model that takes into account zero field splitting of single ion levels;[20] thus, the S = 5/2 Mn[II] ions do not exhibit independent spin behavior.

Furthermore, antiferromagnetic ordering is evident from the peak in the $\chi(T)$ data at 82 K, Figure 5. The critical temperature T_C is defined as the peak in heat capacity, or, equivalently, the peak in $d(\chi T)/dT$, which appears at a temperature somewhat lower than the susceptibility peak.[21,22] The inset to Figure 5 shows that this occurs at T_c = 73 K. This is greater than the 65 K previously reported; the discrepancy is presumably due to impurities in the previous sample.[4] A feature is also evident at 26 K in $\chi(T)$ and in $d\chi/dT$ (vide infra).

The in-phase real, $\chi'(T)$, and out-of-phase complex, $\chi''(T)$, components of ac susceptibility are also characteristic of antiferromagnetic ordering (Figure 6). Both $\chi'(T)$ and $\chi''(T)$
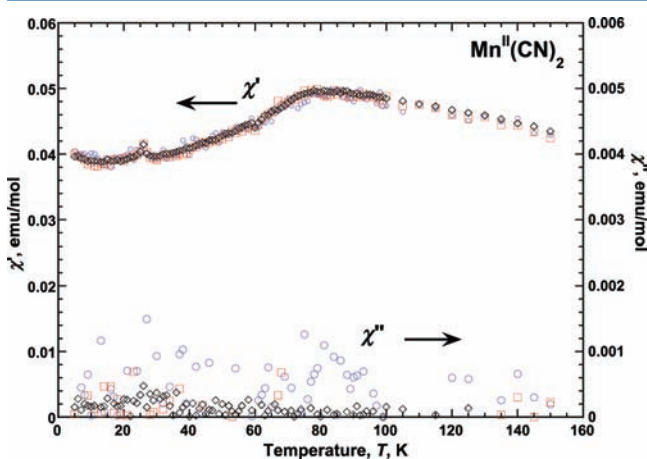
Figure 6. $\chi'(T)$ and $\chi''(T)$ ac susceptibilities for Mn(CN)$_2$ at 33 (×, +), 100 (●, ○), and 1000 (▲, △) Hz.
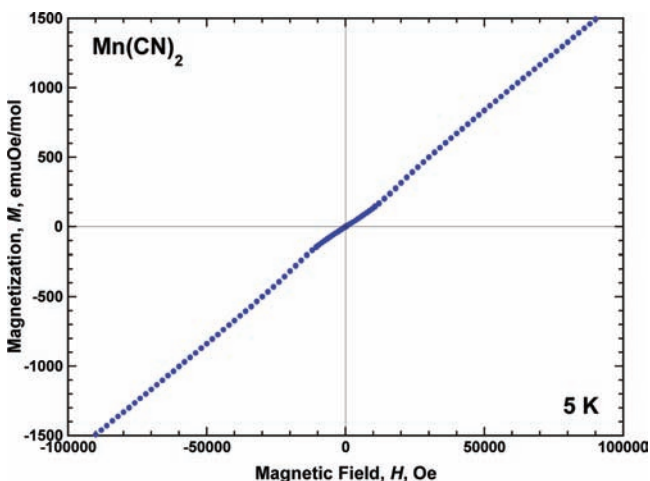
Figure 7. $M(H)$ at 5 K for Mn(CN)$_2$.

are frequency independent, and the peak in the $\chi'(T)$ data occurs at 78 K along with less pronounced peak at 26 K. As expected for antiferromagnetic ordering, there is no response in the $\chi''(T)$ data. As with the $\chi^{-1}(T)$, $\chi(T)$, and $d(\chi T)/dT$ (Figures 4 and 5), the $\chi'(T)$ data (Figure 6) also exhibits a feature at 26 K. This could be due to an impurity, to the

coupling of the two interpenetrating antiferromagnetic lattices, or to some unreacted starting material.[15] Contamination by unreacted starting material seems unlikely, as no evidence could be found for **1** or **2** in the PXRD or IR data, but the possibility of trace amounts cannot be completely excluded, especially since both **1** and **2** have magnetic ordering temperatures ∼26 K.

The 5-K field dependent magnetization, $M(H)$, has a slope at low field of 0.013 emu/mol and a value of 1490 emu Oe/mol at 9 T with no sign of approaching saturation, Figure 7. The value of 1490 emu Oe/mol corresponds to 0.27 spins, greatly reduced from the free ion value, and in accord with antiferromagnetic behavior. The data cannot be modeled by the Brillouin expression.

The nearest neighbor magnetic coupling constant, J, can be estimated by use of the mean field Heisenberg (H = $-2J\sum S_a\cdot S_b$) expression for T_c, eq 1:[22]

$$T_{MF} = \frac{2|J|zS(S+1)}{3k_B}$$ (1)

where z = 4 is the number of nearest neighbors and k_B is Boltzmann's constant. Applicability of the mean field model to a real 3D magnet can be scaled via the nearly ideal Heisenberg antiferromagnet RbMnF$_3$, with z = 6, S = 5/2, and an observed T_C = $0.70T_{MF}$.[23,24] Applying the scale correction factor to Mn(CN)$_2$ implies that it has T_{MF} = 104 K, and therefore J/k_B = −4.4 K.

For an isotropic antiferromagnet, J can also be estimated from the low temperature magnetic susceptibility perpendicular to the axis of magnetization,[22]

$$\chi_\perp(T=0) = \frac{Ng^2\mu_B^2}{4z|J|}$$ (2)

In an isotropic system, the spins rotate perpendicular to an applied field and $\chi = \chi_\perp$; using the value 0.013 emu/mol and assuming g = 2 yields an estimate of J/k_B = −7.2 K. The discrepancy between these two estimates for J may arise from local, random anisotropy at the Mn[II] sites, interactions between the interpenetrating lattices, or the fact that the system may be in a different magnetic phase above and below the observed 26 K anomaly.

■ CONCLUSION

The thermal decomposition of [NEt$_4$]Mn[II]$_3$(CN)$_7$ (**1**) and [NEt$_4$]$_2$Mn[II]$_3$(CN)$_8$ (**2**) leads to the formation of Mn[II](CN)$_2$ that possesses an interpenetrating 3-D diamond lattice framework with Mn[II] ions tetrahedrally bound to orientationally disordered CN⁻. Mn[II](CN)$_2$ magnetically orders as an antiferromagnet below 73 K from $d(\chi T)/dT$ data. This synthetic route provided a higher quality material, as evidenced by its white color, diffraction pattern, and magnetic data with respect to our previously reported synthesis from [PPN]$_2$[Mn[II](CN)$_4$] and [Mn[II](NCMe)$_6$]{B[3,5-C$_6$H$_3$(CF$_3$)$_2$]$_4$}.

■ ASSOCIATED CONTENT

⑤ Supporting Information

Powder X-ray crystallographic CIF file for Mn(CN)$_2$ (CCDC 845910). This material is available free of charge via the Internet at http://pubs.acs.org. This material is also available at Cambridge Crystal Database.

■ AUTHOR INFORMATION

Corresponding Author

*E-mail: jsmiller@chem.utah.edu (J.S.M.); peter.stephens@ sunysb.edu (P.W.S.).

Notes

The authors declare no competing financial interest.

■ REFERENCES

(1) Verdaguer, M.; Girolami, G. S. In *Magnetism - Molecules to Materials*; Miller, J. S., Drillon, M., Eds.; Wiley-VCH: Weinheim, 2005; Vol. 5, p 283. Hashimoto, K.; Ohkoshi, S. *Philos. Trans. R. Soc. London, Ser. A* **1999**, *357*, 2977. Verdaguer, M.; Bleuzen, A.; Marvaud, V.; Vaissermann, J.; Seuleiman, M.; Desplanches, C.; Sciuller, A.; Train, C.; Garde, R.; Gelly, G.; Lomenech, C.; Rosenman, I.; Veillet, P.; Cartier, C.; Villain, F. *Coord. Chem. Rev.* **1999**, *190−192*, 1023.

(2) (a) Ferlay, S.; Mallah, T.; Ouahes, R.; Veillet, P.; Verdaguer, M. *Nature* **1995**, *378*, 701. (b) Dujardin, E.; Ferlay, S.; Phan, X.; Desplanches, C.; Moulin, C. C. D.; Sainctavit, P.; Baudelet, F.; Dartyge, E.; Veillet, P.; Verdaguer, M. *J. Am. Chem. Soc.* **1998**, *120*, 11347. (c) Ferlay, S.; Mallah, T.; Ouahes, R.; Veillet, P.; Verdaguer, M. *Inorg. Chem.* **1999**, *38*, 229. (d) Verdaguer, M.; Bleuzen, A.; Train, C.; Garde, R.; Fabrizi de Biani, F.; Desplanches, C. *Philos. Trans. R. Soc. London, Ser. A* **1999**, *357*, 2959.

(3) (a) Holmes, S. M.; Girolami, G. S. *J. Am. Chem. Soc.* **1999**, *121*, 5593. (b) Hatlevik, Ø.; Buschmann, W. E.; Zhang, J.; Manson, J. L.; Miller, J. S. *Adv. Mater.* **1999**, *11*, 914.

(4) Manson, J. L.; Buschmann, W. E.; Miller, J. S. *Angew. Chem., Int. Ed.* **1998**, *37*, 783.

(5) Manson, J. L.; Buschmann, W. E.; Miller, J. S. *Inorg. Chem.* **2001**, *40*, 1926.

(6) (a) Hoskins, B. F.; Robson, R. *J. Am. Chem. Soc.* **1990**, *112*, 1546. (b) Williams, D. J.; Partin, D. E.; Lincoln, F. J.; Kouvetakis, J.; O'Keefe, M. *J. Solid State Chem.* **1997**, *134*, 164. (c) Reckeweg, O.; Simon, A. Z. *Naturforsch.* **2002**, *57b*, 895.

(7) Beauvais, L. G.; Long, J. A. *J. Am. Chem. Soc.* **2002**, *124*, 12096.

(8) Pinkington, M.; Descurtins, S. *Comp. Coord. Chem. III* **2004**, *7*, 177.

(9) Larionova, J.; Willemin, S.; Donnadieu, B.; Henner, B.; Guérin, C.; Gillon, B.; Goujon, A. *J. Phys. Chem. Solids* **2004**, *65*, 677.

(10) (a) Tomono, K.; Tsunobuchi, Y.; Nakabayashi, K.; Ohkoshi, S.-i. *Inorg. Chem.* **2010**, *49*, 1298. (b) Larionova, J.; Clérac, R.; Donnadieu, B.; Guérin, C. *Chem.—Eur. J.* **2002**, *8*, 2712. (c) Rombaut, G.; Golhen, S.; Ouahab, L.; Mathonière, D.; Kahn, O. *J. Chem. Soc., Dalton Trans.* **2000**, 3609. (d) Larionova, J.; Kahn, O.; Golhen, S.; Ouahab, L.; Clérac, R. *Inorg. Chem.* **1999**, *38*, 3621. (e) Milon, J.; Daniel, M.-C.; Kaiba, A.; Guionneau, P.; Brandèès, S.; Sutter, J.-P. *J. Am. Chem. Soc.* **2007**, *129*, 13872. (f) Tanase, S.; Tuna, F.; Guionneau, P.; Maris, T.; Rombaut, G.; Mathoniere, C.; Andruh, M.; Kahn, O.; Sutter, J.-P. *Inorg. Chem.* **2003**, *42*, 1625. (g) Le Goff, X. F.; Willemin, S.; Coulon, C.; Larionova, J.; Donnadieu, B.; Clérac, R. *Inorg. Chem.* **2004**, *43*, 4784. (h) Larionova, J.; Kahn, O.; Gohlen, S.; Ouahab, L.; Clérac, R. *J. Am. Chem. Soc.* **1999**, *121*, 3349. (i) Mironov, V. S.; Chibotaru, L. F.; Ceulemans, A. *J. Am. Chem. Soc.* **2003**, *125*, 9750.

(11) (a) Sieklucka, B.; Podgajny, R.; Pinkowicz, D.; Nowicka, B.; Korzeniak, T.; Balanda, M.; Wasiutynski, T.; Pelka, R.; Makarewicz, M.; Czapla, M.; Rams, M.; Gawel, B.; Lasocha, W. *CrystEngComm* **2009**, *11*, 2032. (b) Przychodzen, P.; Korzeniak, T.; Podgajny, R.; Sieklucka, B. *Coord. Chem. Rev.* **2006**, *250*, 2234.

(12) (a) Anderson, P. W. *Phys. Rev.* **1950**, *79*, 350. (b) Goodenough, J. B. *J. Phys. Chem. Solids* **1958**, *6*, 287. (c) Kanamori, J. *J. Phys. Chem. Solids* **1959**, *10*, 87.

(13) Her, J.-H.; Stephens., P. W.; Kareis, C. M.; Moore, J. G.; Min, K. S.; Park, J.-W.; Bali, G.; Kennon, B. S.; Miller, J. S. *Inorg. Chem.* **2010**, *49*, 1524.

(14) Kareis, C. M.; Lapidus, S. H.; Her, J.-H.; Stephens, P. W.; Miller, J. S. *J. Am. Chem. Soc.* **2012**, *134*, 2246.

(15) Kareis, C. M.; Her, J.-H.; Stephens, P. W.; Moore, J. G.; Miller, J. S., submitted.

(16) Her, J.-H.; Stephens, P. W.; Kareis, C. M.; Moore, J. G.; Miller, J. S. *Angew. Chem.* **2010**, *49*, 7773.

(17) Brandon, E. J.; Rittenberg, D. K.; Arif, A. M.; Miller, J. S. *Inorg. Chem.* **1998**, *37*, 3376.

(18) Bruker AXS. *TOPAS V4: General profile and structure analysis software for powder diffraction data: User's Manual*; Bruker AXS: Karlsruhe, Germany, 2005. TOPAS-Academic is available at http://www.topas-academic.net.

(19) A small amount of crystalline impurity phase is observed from an analysis of the PXRD data. The crystalline material has a PXRD pattern similar to what would be expected for MnO. MnO, however, orders as an antiferromagnet (T_c = 117 K), and evidence for this is not observed. As with any sample characterized by PXRD, it is not possible to exclude minority amorphous impurity phases.

(20) O'Connor, C. J. *Prog. Inorg. Chem.* **1982**, *29*, 203.

(21) Fisher, M. E. *Philos. Mag.* **1962**, *7*, 1731.

(22) Carlin, R. L. *Magnetochemistry*; Springer-Verlag: 1986; p 121.

(23) de Jongh, L. J.; Miedema, A. R. *Experiments on simple magnetic model systems*; Taylor and Francis: 1974; reprinted from *Adv. Phys.* **1974**, *23*, 1.

(24) Windsor, C. G.; Stevenson, R. W. H. *Proc. Phys. Soc.* **1966**, *87*, 501.